Journal of Ceramic Processing Research. Vol. 23, No. 6, pp. 919~925 (2022)
(Received 26 August 2022, Received in revised form 28 November 2022, Accepted 6 December 2022)
https://doi.org/10.36410/jcpr.2022.23.6.919

J O U R N A L O F
Ceramic Processing Research

Microwave dielectric properties of $Mg_2Ti_{1-x}(Ni_{1/3}Sb_{2/3})_xO_4$ ceramics

Yun Sik Park and Eung Soo Kim*
Department of Advanced Materials Engineering, Kyonggi University, Suwon, Gyeonggi-do 16227, Korea

Dependence of the dielectric properties of $Mg_2Ti_{1-x}(Ni_{1/3}Sb_{2/3})_xO_4$ ($0.025 \le x \le 0.1$) on structural characteristics were investigated at microwave frequencies. For the specimens sintered at 1450 °C for 4 h (single-step sintering), the quality factor (*Qf*) initially increased with increasing $(Ni_{1/3}Sb_{2/3})^{4+}$ content (*x*) up to $x = 0.05$, and then decreased. Highest *Qf* value (182,270 GHz) was obtained for the specimen with $x = 0.05$ sintered through two-step sintering (1450 °C, 10 min followed by 1400 °C, 4 h) owing to its high densification and homogenous microstructure. The quality factor (*Qf*) depends on relative density and bond valence which is dependent on the bond strength and length between oxygen ions and cations in the oxygen octahedron of the crystal structure. The highest bond strength was also confirmed for specimens with $x = 0.05$ based on shifts in the peak position and full width at half maximum of the Raman mode. Overall, $Mg_2Ti_{0.95}(Ni_{1/3}Sb_{2/3})_{0.05}O_4$ ceramics showed high *Qf* (=182,270 GHz), appropriate *K*(=14.13) and adjustable *TCF*(=-48.2 ppm/°C), which are applicable to telecommunication systems and the integration of devices at microwave frequencies.

Key words: Magnesium titanate, Microwave dielectric properties, Quality factor, Two step sintering, Bond valence.

Introduction

With recent advances in wireless and mobile communications, such as fifth-generation (5G) communication and the Internet of Things (IoT), advanced microwave dielectric ceramics are required for various microwave communication systems and the integration of microwave devices. To date, several types of microwave dielectric ceramics such as complex perovskite structure [1], ilmenite structure[2], spinel structure [3], corundum structure [4], rock salt structure [5] compounds and their solid solutions with an appropriate dielectric constant (*K*), high quality factor (*Qf*) and adjustable temperature coefficient of the resonant frequency (*TCF*) have been extensively investigated to achieve device miniaturization, superior cross-coupling selectivity and the integration of microwave devices, respectively [6, 7] Recently, considerable research activities such as chemical substitution and additives for each crystal structure [8-10], crystal structural dependence [11, 12] and processing dependence [13, 14] of dielectric properties at microwave frequencies and so on have been paid to the search for microwave dielectric ceramics with a quality factor (*Qf*) higher than 10^5 GHz to satisfy the demands of 5G and/or next generation communication systems [15].

Because Mg_2TiO_4 ceramics are good candidates for a high quality factor (*Qf*), numerous studies [16-21] for the quality factor (*Qf*) of Mg_2TiO_4 ceramics have been carried out to enhance the dielectric properties at microwave frequencies. Substitution ions with equal in valance for Mg^{2+} and/or Ti^{4+} sites have improved the *Qf* of Mg_2TiO_4 ceramics [17-19], and an enhanced *Qf* of Mg_2TiO_4 has also been achieved by substituting the Ti site with complex ions of $(Mg_{1/3}Sb_{2/3})^{4+}$and $(Mg_xNb_{0.8-0.4x})^{4+}$ [20, 21]. However, most previous studies have reported the quality factor (*Qf*) of Mg_2TiO_4 ceramics depends only on the extrinsic factors, secondary phase, microstructure, and density.

To search for advanced microwave dielectric ceramics with a high quality factor (*Qf*) effectively, the effects of intrinsic factors, structural characteristics, extrinsic factors, microstructure, density, and secondary phases on the quality factor (*Qf*) of microwave dielectric ceramics should be investigated as fundamental research.

According to the previous reports of [14, 22, 23], high densification and effective control of the homogenous microstructure of $BaTiO_3$ were achieved using a two-step sintering (TSS) method, and the dielectric properties were improved.

Therefore, dielectric properties of Mg_2TiO_4 ceramics at microwave frequencies are investigated with complex ion $(Ni_{1/3}Sb_{2/3})^{4+}$ substitution for Ti- site in this study. The dielectric properties of $Mg_2Ti_{1-x}(Ni_{1/3}Sb_{2/3})O_4$ ($0.025 \le x \le 0.1$) at microwave frequencies are affected by both extrinsic and intrinsic factors, which are controlled via the TSS method and complex ion substitution, respectively. The improved dielectric properties of the specimens at microwave frequencies

*Corresponding author:
Tel : +82-31-249-9764
Fax: +82-31-244-6300
E-mail: eskim@kyonggi.ac.kr

are evaluated and analysed quantitatively based on the characteristics of crystal structure via the Rietveld refinement method and Raman spectroscopy.

Experimental Procedures

MgO, Sb_2O_5, TiO_2, and NiO with high purity (99.9%, Kojundo Chemical Laboratory Co., LTD, Japan) were used for the preparation of $Mg_2Ti_{1-x}(Ni_{1/3}Sb_{2/3})_xO_4$ ($0.025 \leq x \leq 0.1$) ceramics as raw materials. For the conventional solid-state reaction, the samples were weighed and milled for 24 h in ethanol media with ZrO_2 balls. Calcination was carried out at 1150 °C for 4 h, re-milled and then dried. The dried mixtures were pressed in a die with a diameter of 12 mm under 1500 kg/cm^2 isostatically. The green bodies were sintered at 1450 °C for 4 h in air using a single-step sintering (SSS) method.

Generally, densification process and grain growth process which are dependent on the specific temperature range, are occurred in the sintering process of ceramics. High densification and homogeneous microstructure of ceramics could be obtained from the effective control of densification process and grain growth process, respectively. Two-step sintering (TSS) method was employed in this study to obtain the homogeneous microstructure with high densification of ceramics.

For TSS method, the pressed specimens of $Mg_2Ti_{0.95}(Ni_{1/3}Sb_{2/3})_{0.05}O_4$ were sintered at 1450 °C for 10 min in the first stage (T_1), and then sintered at 1400 °C for 4 h in the second stage (T_2). To enable comparison with the specimens using the SSS method, the holding time at T_2 was 4 h. The rates of heating and cooling were 5 °C/min in the range of 25 °C to T_1 (1450 °C) and 25 °C/min in the range of T_1 to T_2, respectively.

X-ray powder diffraction (XRD; D/Max-3C, Rigaku, Japan) was used for examination of crystalline phases over the range of 2θ = 10°–65°. From the Rietveld refinements of XRD patterns, the crystal structural characteristics of the sintered specimens were obtained using the WinPLOTR program [24]. Details of the structural characteristics were also obtained by Raman spectra (T64000, Horiba Jobin Yvon, France) with an Ar^+ ion laser (wavelength: 514 nm). The microstructural characteristics were examined using scanning electron microscopy (SEM; JSM-6500F, JEOL, Japan).

Calculations of the relative densities were performed from apparent densities obtained from Archimedes method and the theoretical density obtained from Rietveld refinements. Hakki and Coleman method with pararell plate of silver connected to network analyser (E5071C, Agilent Technologies, USA) applied to measure the dielectric constant (K) and quality factor (Qf) of the specimens from 9 to 11 GHz [25]. For the temperature range from 25 °C to 80 °C, the cavity (Murata MFG Co., LTD, Japan) method was applied to measure thermal stability of the resonant frequency (TCF) [26].

Results and Discussion

Two-step sintering (TSS) method

To realize high densification with a homogenous microstructure in $Mg_2Ti_{0.95}(Ni_{1/3}Sb_{2/3})_{0.05}O_4$ ceramics, a TSS method comprising individual steps of grain growth and densification was performed. At the first sintering temperature, T_1, the relative density of the specimens should be greater than 75% of the theoretical density, and T_1 should be a higher temperature than that of the second sintering step, T_2, to ensure sufficient driving force for high densification in the second sintering step [27]. The relative density of the sintered specimens is calculated as a function of time according to Eq. (1) [28]:

$$\rho(t) = \frac{\left(1+\frac{L_f - L_o}{L_o}\right)\left(1+\frac{\phi_f - \phi_0}{\phi_0}\right)^2}{\left(1+\frac{\Delta L(t)}{L_o}\right)\left(1+\alpha\frac{\Delta L(t)}{L_o}\right)^2}\rho_f \quad (1)$$

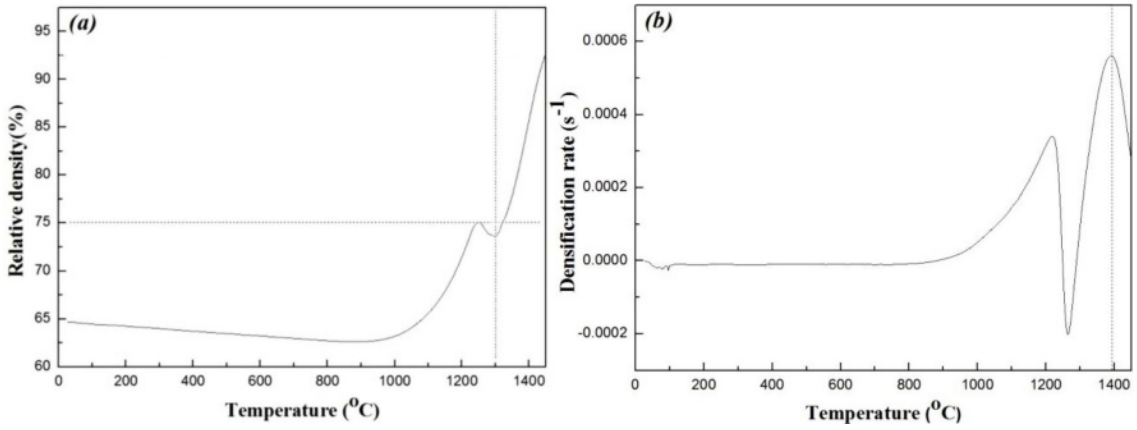

Fig. 1. (a) Relative density and (b) densification rate of $Mg_2Ti_{0.95}(Ni_{1/3}Sb_{2/3})_{0.05}O_4$ as a function of the sintering temperature.

where L_f and L_o are the final and initial lengths, respectively; ϕ_f and ϕ_0 are the mean diameters of the specimen each at the final and initial stages, respectively; and ρ_f is the final relative density. From the dilatometry data, the shrinkage can be calculated as a time function ($\Delta L(t)$).

As shown in Fig. 1(a), a relative density exceeding 75% of the theoretical density was obtained for specimens in the first-step at temperatures above 1300 °C. Therefore, the first-step sintering temperature, T_1, for $Mg_2Ti_{1-x}(Ni_{1/3}Sb_{2/3})_xO_4$ was set above 1300 °C.

The second-step sintering temperature, T_2, should be set at the temperature that has the highest densification rate [29]. The densification rate of $Mg_2Ti_{1-x}(Ni_{1/3}Sb_{2/3})_xO_4$ can be calculated by differentiation of Eq. (1), as expressed in Eq. (2).

$$\beta = \left(1+\frac{L_f-L_0}{L_0}\right)\left(1+\frac{\phi_f-\phi_0}{\phi_0}\right)^2 \rho_f$$

$$\frac{d\rho}{dt} = \frac{dL}{L_o dt}\left(2-\frac{\Delta L(t)}{L_o}\right)^{-2} \times \left\{1-\alpha\left(\frac{dL}{L_o dt}-1\right)\right\}^{-2}$$

$$+2\alpha\frac{dL}{L_o dt}\times\left\{1-\alpha\left(\frac{dL}{L_o dt}-1\right)\right\}^{-3} \times \left(2-\frac{\Delta L(t)}{L_o}\right)^{-1} \times \beta \quad (2)$$

As shown in Fig. 1(b), T_2 is set at 1400 °C because this temperature provides the highest densification rate. For consideration of the TSS method schedule, T_1 should also be set above 1400 °C; therefore, T_1 was set to as 1450 °C.

However, Fig. 1(b) shows a remarkable decrease in the densification rate at 1250 °C. This result may be related to the thermal decomposition of $Mg_2Ti_{1-x}(Ni_{1/3}Sb_{2/3})_xO_4$ to MgO and $Mg_2Ti_{1-x}(Ni_{1/3}Sb_{2/3})_xO_4$ at high temperatures [30]. Thus the details of thermal decomposition should be studied sooner or later.

Physical and dielectric properties of $Mg_2Ti_{1-x}(Ni_{1/3}Sb_{2/3})_xO_4$ ceramics at microwave frequencies

The XRD patterns of the specimens sintered using the SSS method and TSS method are shown in Fig. 2. The entire range of compositions showed the inverse-spinel structure with single phase. The XRD peaks at 2θ = 35°–36° shifted toward lower angles with an increase in the $(Ni_{1/3}Sb_{2/3})^{4+}$ content (x), because the ionic radius of $(Ni_{1/3}Sb_{2/3})^{4+}$ (0.64 Å) is larger than that of Ti^{4+} (0.605 Å) [31]. Volume of unit-cell increased with the number of substitutions from these results.

Fig. 3(a)-(c) show SEM micrographs of the specimens sintered at 1450 °C for 4 h in the SSS method. With an increase in the $(Ni_{1/3}Sb_{2/3})^{4+}$ content (x) from x = 0.05 to x = 0.1, the grain size of the specimens gradually decreased. Moreover, the SEM micrograph of the specimen sintered at 1400 °C for 4 h (Fig. 3(d)) shows a small grain size and heterogeneous

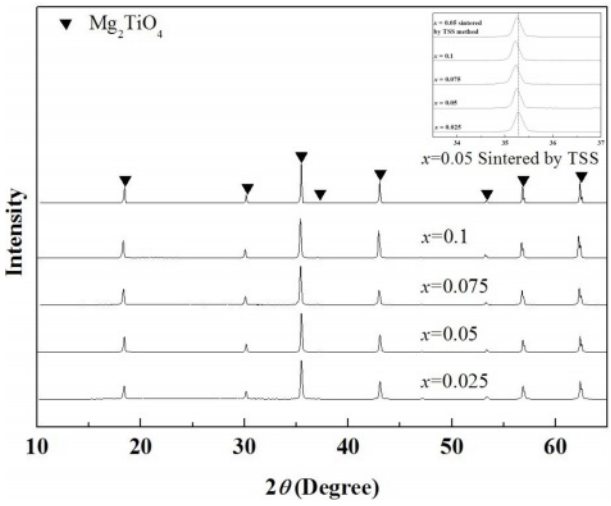

Fig. 2. X-ray diffraction patterns of $Mg_2Ti_{1-x}(Ni_{1/3}Sb_{2/3})_xO_4$ ($0.025 \leq x \leq 0.1$) specimens sintered at 1450 °C for 4 h and $Mg_2Ti_{0.95}(Ni_{1/3}Sb_{2/3})_{0.05}O_4$ specimens sintered at 1450 °C for 10 min followed by 1400 °C for 4 h.

microstructure. A remarkably low *Qf* is achieved from the microstructural characteristics of the $Mg_2Ti_{0.95}(Ni_{1/3}Sb_{2/3})_{0.05}O_4$ ceramic sintered at 1400 °C for 4h. These results are in good agreement with the variation in the *Qf* of the sintered specimens with the $(Ni_{1/3}Sb_{2/3})^{4+}$ content, as confirmed in Table 1 and Fig. 4. On the other hand, the $Mg_2Ti_{0.95}(Ni_{1/3}Sb_{2/3})_{0.05}O_4$ ceramics sintered using the TSS method (Fig. 3(e)) show a small grain size and homogeneous microstructure owing to the suppression of grain growth and enhanced densification during sintering [27]. However, this result contradicts that the specimens sintered by the TSS method showed higher *Qf* value than that of specimens sintered by the SSS method.

The dependence of *Qf* on the sintering conditions and compositions of the specimens is clearly shown in Fig. 4. According to the previous report [32], the effect of extrinsic factors cannot be fully explained by the *Qf* changes of the sintered specimens alone because the relative density higher than 97% of theoretical density can be passed up the effect of extrinsic factors. Therefore, the *Qf* of sintered specimens should be evaluated based on intrinsic factors of structural characteristics rather than extrinsic factors of micro-structural characteristics.

Rietveld refinement is an effective method for obtaining the structural characteristics of sintered specimens. Table 2 summarizes the reliabilities of the Rietveld refinements performed using the XRD patterns of $Mg_2Ti_{1-x}(Ni_{1/3}Sb_{2/3})_xO_4$ ceramic specimens. All of the sintered specimens showed Bragg R-factors (R_{Bragg}) and the goodness-of-fits (*GoF*) of less than approximately 8 and 2, respectively.

Figure 5 shows the typical Rietveld refinement pattern of $Mg_2Ti_{0.95}(Ni_{1/3}Sb_{2/3})_{0.05}O_4$ sintered at 1450 °C for 4 h. Good matches were confirmed between the

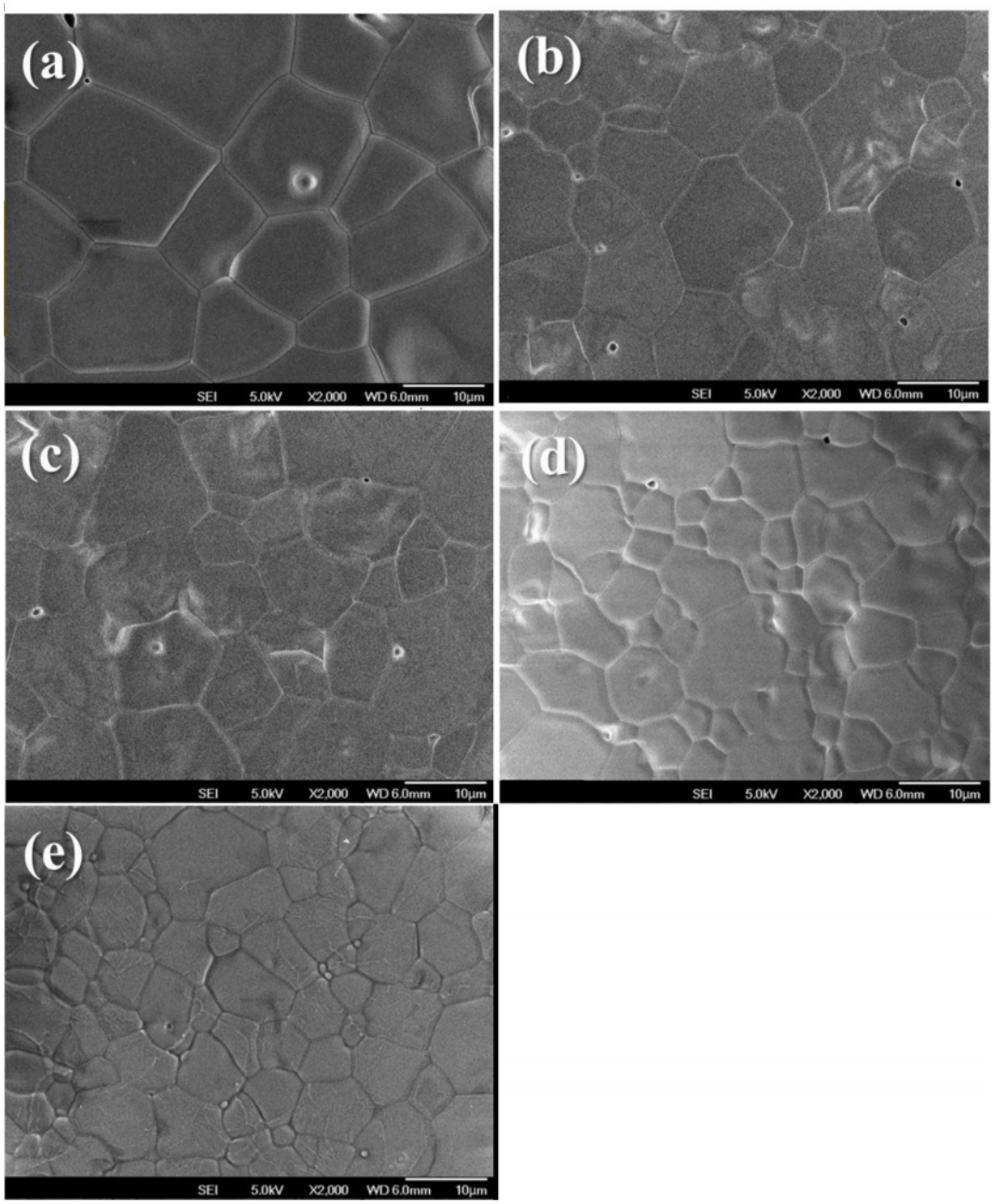

Fig. 3. SEM micrographs of $Mg_2Ti_{1-x}(Ni_{1/3}Sb_{2/3})_xO_4$ ($0.025 \le x \le 0.1$) specimens sintered at 1450 °C for 4 h: (a) $x = 0.05$, (b) $x = 0.075$, (c) $x = 0.1$; SEM micrographs of $Mg_2Ti_{0.95}(Ni_{1/3}Sb_{2/3})_{0.05}O_4$ specimens sintered at (d) 1400 °C for 4 h and (e) 1450 °C for 10 min followed by 1400 °C for 4 h. (scale bars = 10 μm)

Table 1. Apparent density, relative density, quality factor, dielectric constant and temperature coefficient of the resonant frequency of sintered $Mg_2Ti_{1-x}(Ni_{1/3}Sb_{2/3})_xO_4$ ($0.025 \le x \le 0.1$) specimens.

x (mol)	Apparent density (g/cm^3)	Relative density (%)	Quality factor, Qf (GHz)	Dielectric constant, K	Temperature coefficient of the resonant frequency, TCF (ppm/°C)
0.025	3.4762	96.7276	164,070	14.35	-46.51
0.05	3.5432	96.8082	168,151	14.3	-47.23
0.075	3.5703	96.2669	137,042	14.14	-48.71
0.1	3.5323	95.2209	126,183	13.55	-49.1
0.05 by TSS	3.5074	97.3031	182,276	14.17	-48.21

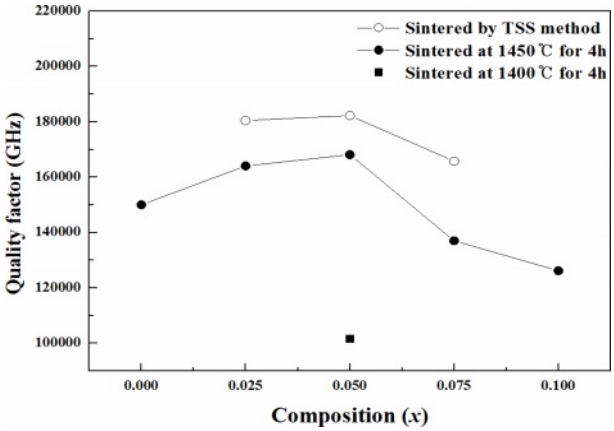

Fig. 4. Dependence of *Qf* on the sintering conditions and composition of $Mg_2Ti_{1-x}(Ni_{1/3}Sb_{2/3})_xO_4$ ($0.025 \le x \le 0.1$) ceramics.

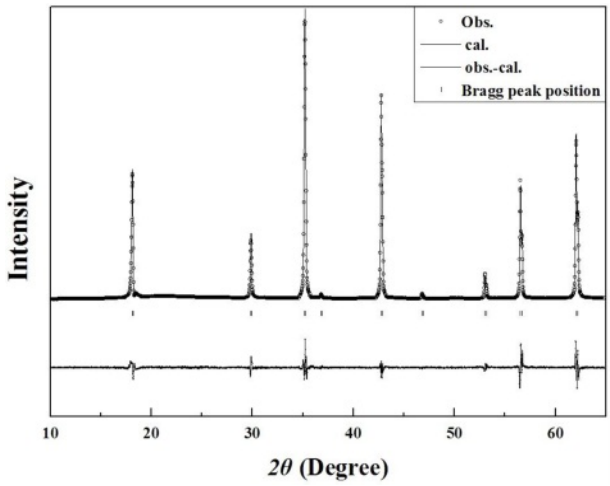

Fig. 5. Rietveld refinement patterns of $Mg_2Ti_{0.95}(Ni_{1/3}Sb_{2/3})_{0.05}O_4$ specimens sintered at 1450 °C for 4 h.

observed XRD data (dots) and the refinement data (solid lines). From Rietveld refinement, crystallographic data; the volume of unit-cell, lattice parameters and bond length of the cation-oxygen ions can be obtained. The volume of unit-cell increased with increasing $(Ni_{1/3}Sb_{2/3})^{4+}$ content (x) because the ionic radii of $(Ni_{1/3}Sb_{2/3})^{4+}$ (0.64 Å) [31] is larger than that of Ti^{4+} (0.605 Å) [31]. In addition, the bond characteristics on the cation-oxygen ions of each oxygen tetrahedron and octahedron were quantified using the bond valence, which is an adequate indicator of bond characteristics for the evaluation of structural characteristics [33]. The bond valence is expressed by Eqs. (3) and (4) [34, 35]:

$$v_{ij} = \exp[(R_{ij} - d_{ij})/b], \quad (3)$$

$$V_{ij} = \Sigma v_{ij}, \quad (4)$$

where R_{ij} is the bond valence parameter, which was reported by Brese et al. [36]; d_{ij} is the bond length (cation-oxygen ion) in the oxygen polyhedron obtained from Rietveld refinement; and b is 0.37 Å as a universal constant.

The effects of $(Ni_{1/3}Sb_{2/3})^{4+}$ substitution for Ti^{4+} and the TSS method were evaluated based on the bond valence. Because a high bond valence indicates high bond strength, the bond valence is proportional to the *Qf* of the sintered specimens. As shown in Fig. 6, the results show a good correlation between *Qf* and the

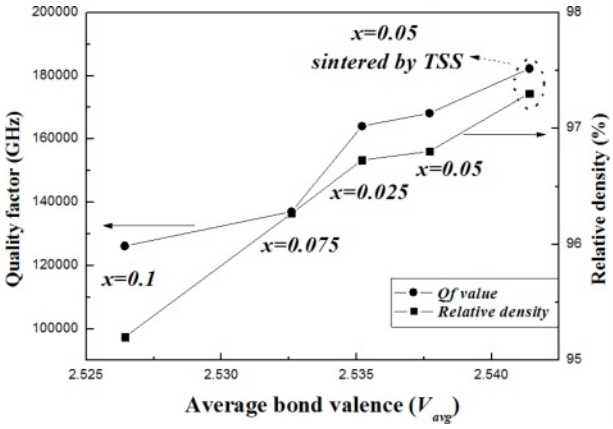

Fig. 6. Dependence of *Qf* and the relative density on the average bond valence of $Mg_2Ti_{1-x}(Ni_{1/3}Sb_{2/3})_xO_4$ specimens sintered at 1450 °C for 4 h and those sintered using the TSS method.

bond valence. *Qf* value of the specimen with x = 0.05 mol sintered by the TSS method was higher than that of the other sintered specimens.

Figure 7 shows Raman spectra and *Qf* of the specimens sintered at 1450 °C for 4 h. The Raman spectra can also be used to identify bond characteristics such as the cation ordering and chemical bond strength

Table 2. Lattice parameter, unit cell volume, and structural characteristic data for sintered $Mg_2Ti_{1-x}(Ni_{1/3}Sb_{2/3})_xO_4$ ($0.025 \le x \le 0.1$) specimens.

x (mol)	Lattice parameter (Å)	Unit cell Volume (Å^3)	Bond length		Bond valence				GoF
			$d_{T\text{-}O}$ (Å)	$d_{M\text{-}O}$ (Å)	V_T	$V_{M\text{-}Mg}$	$V_{M\text{-}Ti}$	V_{avg}	
0.025	8.4429	601.8364	1.9688	2.0344	1.8981	2.3846	3.3323	2.5352	3
0.05	8.4489	602.9635	1.9699	2.0340	1.8928	2.3870	3.3334	2.5377	1.9
0.075	8.4502	603.409	1.9681	2.3607	1.9019	2.3739	3.3220	2.5326	2.8
0.1	8.4544	604.298	1.9300	2.0580	2.1080	2.2373	3.1374	2.4942	1.3
0.05 by TSS	8.4479	602.909	1.9874	2.0277	1.8053	2.4282	3.3908	2.5414	2.7

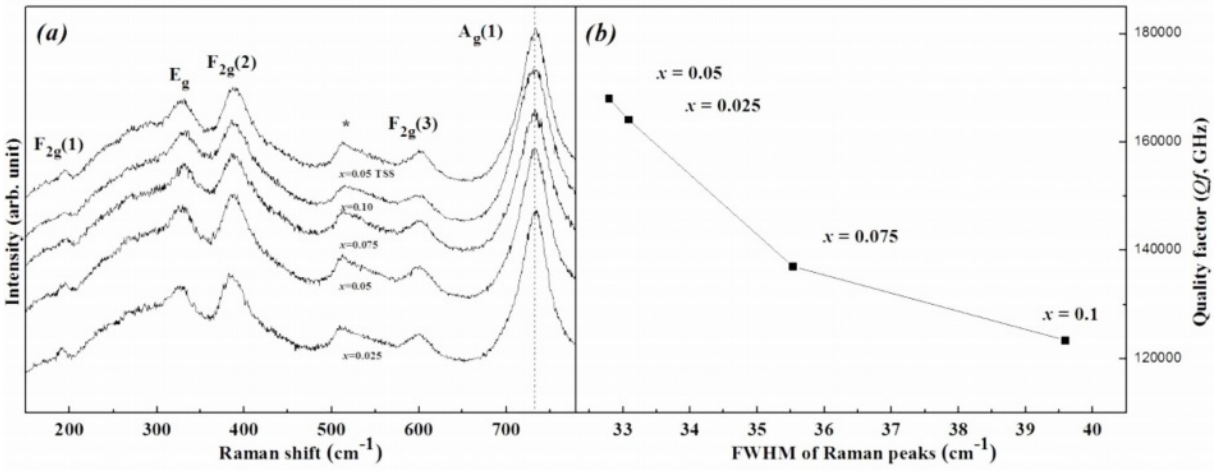

Fig. 7. (a) Raman peak shifts and (b) relationship between the FWHM values of the $A_g(1)$ Raman mode and *Qf* of $Mg_2Ti_{1-x}(Ni_{1/3}Sb_{2/3})_xO_4$ ($0.025 \leq x \leq 0.1$) specimens sintered at 1450 °C for 4 h.

[37, 38]. The inverse-spinel structure consists of five Raman modes ($A_g(1) + E_g + 3F_{2g}$) [39]. Although the specific atomic motions are assigned in the spinel lattice for the Raman-active vibrations, especially the A_{1g} mode was inconsistent in previous reports [40], the A_{1g} mode is commonly relevant to the cation-oxygen bond strength in the tetrahedra. According to Barpanda [41], each tetrahedron of the inverse-spinel structure shares an oxygen with other octahedra, and thus the cation-oxygen bond in the tetrahedron can influence the bonding force in the octahedra through a change in the oxygen position along the connections between each oxygen polyhedron. Meanwhile, according to Gupta [42], $\nu_1 = \nu(A_{1g})$, which indicates the cation-oxygen bond stretching force constant of an octahedron and is related to the chemical bond strength, is determined as that of Mg-O for the value of ν_1. Thereby, among the five Raman modes, $A_g(1)$ involves not only the Mg-O bond stretching mode in the tetrahedra but also the deformation of other bonds in the octahedra. Generally, the frequency of ν_1 is decreased with increasing atomic weight of the cation [43]. Therefore, the peaks of the $A_g(1)$ mode decreased with amount of substitutions because the atomic weight of $(Ni_{1/3}Sb_{2/3})^{4+}$ is larger than Ti^{4+}. Although there was no compositional change, the specimen with $x = 0.05$ sintered using the TSS method showed higher peak frequency than that of specimens sintered at 1450 °C for 4 h in the SSS method. This result indicates that the bond strength of specimens was enhanced by the TSS method.

Table 3 summarizes the relationship between the full width at half maximum (FWHM) of the Raman peak and the *Qf* of the specimens. For specimens with a well-ordered structure, the Raman peaks showed the narrowest FWHM values. Because the degree of cation ordering is also an indicator of the *Qf* of the sintered specimens, the peak of the specimen with $x = 0.05$ showed the narrowest FHWM.

Table 3. Raman spectroscopic data for sintered $Mg_2Ti_{1-x}(Ni_{1/3}Sb_{2/3})_xO_4$ ($0.025 \leq x \leq 0.1$) specimens.

x (mol)	Raman shift (cm^{-1})	FWHM of Raman peak
0.025	732.474	33.0742
0.05	732.3514	32.7880
0.075	732.3358	35.5294
0.1	731.8476	39.5866
0.05 by TSS	732.8841	34.5260

Conclusions

The dielectric properties of $Mg_2Ti_{1-x}(Ni_{1/3}Sb_{2/3})_xO_4$ ($0.025 \leq x \leq 0.1$) were investigated at microwave frequencies.

For the specimens obtained through single-step sintering (1450° C for 4 h), the quality factor (*Qf*) increased initially up to $x = 0.05$ with the $(Ni_{1/3}Sb_{2/3})^{4+}$ content (x) and then decreased. For the specimens with $x = 0.05$ obtained through two-step sintering (1450 °C for 10 min followed by 1400 °C for 4 h), the quality factor (*Qf*) was 182,270 GHz, while that of specimens obtained through the single-step sintering method (1450° C for 4 h) showed 168,150 GHz because of the high densification and homogenous microstructure achieved with two-step sintering.

Average bond valences of the Ti-sites of $Mg_2Ti_{1-x}(Ni_{1/3}Sb_{2/3})_xO_4$ were evaluated on the basis of structural characteristics obtained from the Rietveld refinement data of sintered specimens. The average bond valences of Ti-sites of the specimens decreased with increasing $(Ni_{1/3}Sb_{2/3})^{4+}$ content (x). The specimens with $x = 0.05$ obtained using two-step sintering showed the average bond valence of the Ti-site higher than that of the specimens obtained using the single-step sintering

method. The variation in the average bond valence characteristics with the $(Ni_{1/3}Sb_{2/3})^{4+}$ content was also confirmed by changes in the shifted peak position and full width at half maximum of the Raman mode in the Raman spectra. Average bond valence of the Ti-sites and the relative density strongly affected to the quality factor (Qf) of the specimens.

Acknowledgements

This work was supported by Kyonggi University Research Grant 2018.

References

1. C. Li, Y. You, Y. You and C. Kuo, J. Aust. Ceram. Soc. 57[3] (2021) 983-992.
2. Z. Fang, H. Yang, H. Yang, Z. Xiong, X. Zhang, P. Zhao and B. Tang, Ceram. Int. 47[15] (2021) 21388-21397.
3. S. Rabha and P. Dobbidi, J. Mater. Sci.: Mater. Electron., 30[15] (2019) 14600-14610.
4. E.S. Kim and J.M. Kim, J. Korean. Ceram. Soc. 58[5] (2021) 583-589.
5. G.G. Yao, J.X. Yan, J.J. Tan, C.J. Pei, P. Liu, H.W. Zhang and D.W. Wang, J. Eur. Ceram. Soc. 41[13] (2021) 6490-6494.
6. M.T. Sebastian, R. Ubic, and H. Jantunen, Int. Mate. Rev. 60[7] (2015) 392-412.
7. Q. Dai, R. Zuo, Y. Xu and L. He, J. Eur. Ceram. Soc. 40[2] (2020) 376-380.
8. K. Cheng, C. Li, C. Yin, Y. Tang, Y. Sun and L. Fang J. Eur. Ceram. Soc. 39[13] (2019) 3738-3743.
9. S. Uddin, A. Zaman, I. Rasool, S. Akbar, M. Kamran, N. Mehboob, A. Ali, A. Ahmad, M.F. Nasir and Z. Igbai, J. Ceram. Process. Res. 21[6] (2020) 745-750.
10. Z. Xu, L. Li, S. Yu, M. Du and W. Luo, J. Alloy. Comp. 802 (2019) 1-5.
11. H. Li, P. Zhang, S. Yu, H. Yang, B. Tang, F. Li and S. Zhang, Ceram. Int. 45[9] (2019) 11639-11647.
12. H.J. Jo and E.S. Kim, J. Eur. Ceram. Soc. 36[6] (2016) 1399-1405.
13. G.G. Yao, J. Ceram. Process. Res. 16[1] (2015) 41-44.
14. G. Dong, S. Ma, J. Du, and J. Cui, Ceram. Int. 35[5] (2009) 2069-2075.
15. T. Yu, T. Luo, Q. Yang, H. Feng, H. Yu, and J. Liu, J. Mater. Sci.: Mater. Electron. 32[8] (2021) 2547-2556.
16. A. Belous, O. Ovchar, D. Durilin, M.M. Krzmanc, M. Valant, and D. Suvorov, J. Am. Ceram. Soc. 89[11] (2006) 3441-3445.
17. C.L. Huang and J.Y. Chen, J. Am. Ceram. Soc. 92[3] (2009) 675-678.
18. C.L. Huang and C.E. Ho, Int. J. Appl. Ceram. Technol. 7[S1] (2010) E163-E169.
19. C.L. Huang and J.Y. Chen, J. Am. Ceram. Soc. 92[2] (2009) 379-383.
20. S.H. Kim and E.S. Kim, Ceram. Int. 42[13] (2016) 15035-15040.
21. S.H. Kim and E.S. Kim, Ceram. Int. 43[1] (2017) S321-325.
22. A.C. Caballero, J.F. Fernandez, C. Moure, P. Duran, J. Eur. Ceram. Soc. 17[4] (1997) 513-523.
23. A.C. Caballero, J.F. Fernandez, C. Moure, P. Duran, and Y.M. Chiang, J. Am. Ceram. Soc. 81[4] (1998) 939-944.
24. T. Roisnel and F.R. Carvajal, Mater. Sci. Forum. 378-381[1] (2001) 118-123.
25. B.W. Hakki and P.D. Coleman, Microw. Theory. Technol. 8[4] (1960) 402-410.
26. T. Nishikawa, K. Wakino, H. Tamura, H. Tanaka, and Y. Ishikawa, Microw. Symp. Dig. 87[2] (1987) 277-280.
27. I.W. Chen and X.H. Wang, Nature 404[677] (2000) 168-171.
28. D. Lance, J. Eur. Ceram. Soc. 24[9] (2004) 2749-2761.
29. C.J. Wang, C.Y. Huang, and Y.C. Wu, Ceram. Int. 35[4] (2009) 1467-1472.
30. M.A. Petrova, G.A. Mikirticheva, A.S. Novikova, and V. F. Popova, J. Mater. Res. 12[10] (1997) 2584-2588.
31. R.D. Shannon, Acta. Cryst. A 32[5] (1976) 751-767.
32. D.M. Iddles, A.J. Bell, and A.J. Moulson, J. Mat. Sci. 27[23] (1992) 6303-6310.
33. J. Li, Y. Han, T. Qiu, and C. Jin, Mater. Res. Bull. 47[9] (2012) 2375-2379.
34. I.D. Brown and D. Altermatt, Acta. Crystallogr. B 41[4] (1985) 244-247.
35. I.D Brown and K.K. Wu, Acta. Crystallogr. B 32[7] (1976) 1957-1959.
36. N.E. Brese and M. O'Keeffe, Acta. Crystallogr. B 47[2] (1991) 192-197.
37. E.S. Kim and S.N. Seo, J. Ceram. Soc. Jpn. 116[5] (2008) 619-623.
38. C.T. Chia, Y.C. Chen, H.F. Cheng and I.N. Lin, J. Appl. Phys. 94[5] (2003) 3360-3364.
39. S. Kumar, R. Kumar, B.H. Koo, H. Choi, D.U. Kim, and C.G. Lee, J. Ceram. Soc. Jpn. 117[5] (2009) 689-692.
40. D. Lenaz and V. Lughi, Am. Mineral. 102[2] (2017) 327-332.
41. P. Barpanda, S.K. Behera, P.K. Gupta, S.K. Pratihar, and S. Bhattacharya, J. Eur. Ceram. Soc. 26[13] (2006) 2603-2609.
42. H. C. Gupta, A. Parashar, V. B. Gupta and B.B. Tripathi, Phys. Stat. Sol. 160[1] (1990) K19-24.
43. D.J. Kim, J.W. Jang, and H.L. Lee, J. Am. Ceram. Soc. 80[6] (1997) 1453-1461.